Available online at www.sciencedirect.com

ScienceDirect

Procedia Engineering 00 (2017) 000–000

SAND2017-3769C

Procedia Engineering

www.elsevier.com/locate/procedia

DYMAT 23rd Technical Meeting

Dynamic Fracture of Ductile Materials

High Strain Rate Tensile Response of A570 and 4140 Steel

Brett Sanborn[a]*, Bo Song[a], Andrew Thompson[a], Blake Reece[a], Stephen Attaway[a]

[a] *Sandia National Laboratories, 1515 Eubank SE, Albuquerque, NM 87122, USA*

Abstract

Steel grades such as A570 and AISI 4140 are often used for applications where high rate or impact loading may occur. A570 is a hot-rolled carbon steel that is used where a high strength to weight ratio is desired. A grade such as AISI 4140 offers decent corrosion resistance due to higher chromium and molybdenum content and is commonly used in firearm parts, pressurized gas tubes, and structural tubing for roll cages. In these scenarios, the material may undergo high rate loading. Thus, material properties including failure and fracture response at relevant loading rates must be understood so that numerical simulations of impact events accurately capture the deformation and failure/fracture behavior of the involved materials. In this study, the high strain rate tensile response of A570 and 4140 steel are investigated. An increase in yield strength of approximately 28% was observed for 4140 steel when comparing 0.001 s^{-1} strain rate to 3000 s^{-1} experiments. A570 showed an increase in yield strength of approximately 52% when the strain rate increased from quasi-static to 2750 s^{-1}. Effects on true stress and strain at failure for the two materials are also discussed.

Peer-review under responsibility of [NAME OF THE ORGANIZATION].

Keywords: A570 steel, 4140 steel, Kolsky bar, strain rate, stress-strain curve, dynamic tension

* Corresponding author. Tel.: 1-505-845-1087
E-mail address: bsanbor@sandia.gov

Peer-review under responsibility of the scientific committee of the International Conference on Dynamic Fracture of Ductile Materials.

1. Introduction

American Society for Testing and Materials (ASTM) A570 steel is a hot-rolled carbon steel that is used in a variety of applications where a relatively high strength to weight ratio is desired. American Iron and Steel Institute (AISI) 4140 steel provides good corrosion resistance due to higher chromium and molybdenum content. Typical applications for 4140 steel are firearm parts, pressurized gas tubes, and structural tubing for roll cages. In each of these applications, the material may be subjected to high speed or impact loading, which necessitates that the high strain rate properties are investigated, thereby allowing for improved design and simulation of blast or impact events.

The Kolsky tension bar (also called split Hopkinson tension bar) is the primary method to determine the tensile stress-strain response of materials at elevated strain rates in the range of about 500-5000 s^{-1}. Kolsky tension bars have been used extensively in the literature to study the high strain rate response of materials. In general, valid tension bar experiments are more difficult to achieve compared to Kolsky compression bar experiments. One concern with Kolsky tension bar experiments is producing constant strain rate deformation, which is usually achieved through changing the shape of the loading pulse. Most tension bars in existence use a hollow tube striker based on Ogawa's 1984 [1] design that impacts a flange on the end of the incident bar. However, this method makes it difficult to apply pulse shaping techniques to change the shape of the incident pulse. Newer designs use a solid cylindrical striker impacting an end cap attached to the open end of a gun barrel [2]. In the current study, an incident bar was threaded into the other end of the gun barrel, which made the gun barrel act as a portion of load transfer train. Conventional pulse shaping methods that are used in compression may be easily employed using this method compared to the flanged incident bar and tube striker. Other experimental challenges exist such as a pseudo-stress peak in the stress-strain curve due to poor contact between the specimen and bar ends. This was mitigated by Song et al. [3] by adding lock nuts between the specimen and bar to ensure good contact, and thus has been adopted in the current study. The third experimental concern commonly found in tension bar experiments is the accuracy of the strain measurement of the sample but has recently been improved via implementing a dual detector linear laser setup to accurately track the incident and transmission bar ends separately [4]; such a setup has been included in the current study. Finally, the true stress-strain behavior is difficult to quantify after necking occurs in tensile Kolsky bar experiments [5]. To circumvent these concerns in the current study, the specimens were examined after failure occurred and the true stress and strain at failure were quantified using the Bridgman correction [6-8].

In this study, the dynamic tensile stress-strain responses of A570 and 4140 steel are investigated using a Kolsky tension bar at strain rates of approximately 500, 1500, and 3000 s^{-1}. Yield and ultimate stress values are compared to quasi-static values. The true-stress true-strain behavior at failure was examined using the Bridgman correction.

2. Materials and Methods

A570 and 4140 steels were subjected to high strain rate tension at strain rates of 500, 1500, and 3000 s^{-1}. The number of specimens for each material type and strain rate are shown in Table 1. Both specimen types had a gage section that was 3.18 mm in diameter and 6.35 mm long. The tensile specimens of 4140 steel were machined from a cylindrical rod while A570 were machined from a plate. Since the Kolsky tension bar used in this study had 1/2"-20 threads at the ends of the incident and transmission bars to hold the specimen ends, dumbbell-shaped specimens as shown in Fig. 1a were used for 4140 specimens. Due to thickness restrictions on the A570 plate, specimens were machined with 1/4"-20 threaded ends, as shown in Fig. 1b. Due to the dissimilar threads, a pair of adapters were designed, as shown in Fig. 2, to be mounted between the 1/2"-20 bars and the 1/4"-20 A570 specimens.

Table 1. Number of specimens at each condition

Strain Rate (s^{-1})	A570 steel (Number of Samples)	4140 Steel (Number of Samples)
500	3	3
1500	4	3
~3000	3	3

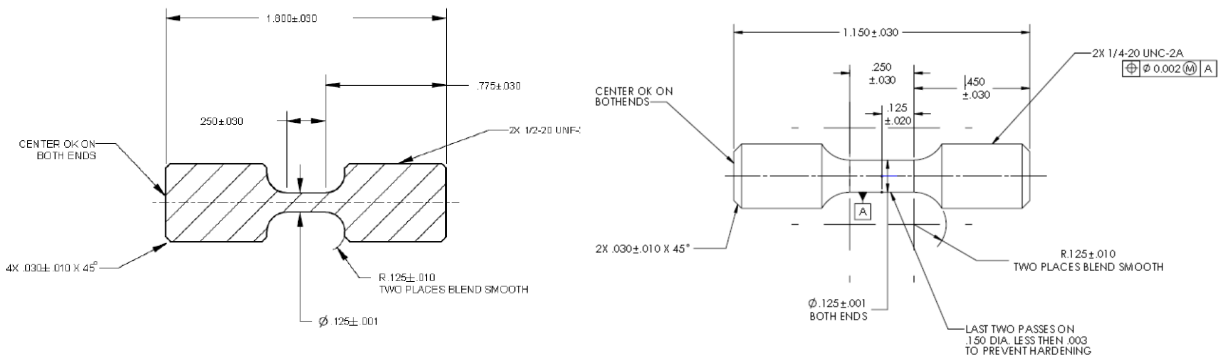

Figure 1. a) Design of 4140 specimens, b) Design of A570 specimens. (All dimensions are in inches)

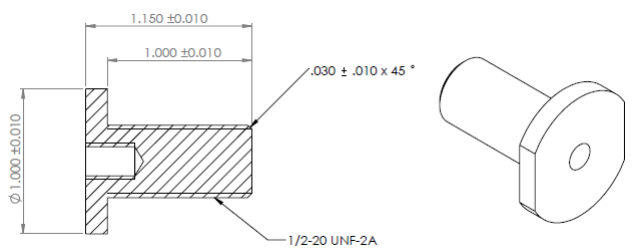

Figure 2. Adapters for A570 specimens

A Kolsky tension bar was used to apply dynamic tensile loading to the steel specimens based on the design presented in [2], as shown in Fig. 3, uses pressurized gas to fire a solid steel striker down a hollow gun barrel. The steel striker impacts the pulse shaper located on an end cap threaded onto the end of the gun barrel. Upon impact, the pulse shaper is compressed. A shaped tensile pulse is generated in the gun barrel and then transferred into the solid 1”-diameter C300 maraging steel incident bar through a coupler. The pulse propagates along the incident bar before reaching the specimen. Upon reaching the specimen interface, the specimen is loaded in tension whereupon part of the pulse is reflected back into the incident bar while the remainder is transmitted through the specimen into the transmission bar. A high-speed, dual photodetector linear laser system is placed at the specimen interface to accurately track the motion of the incident and transmission bar ends [4]. The primary benefit of using a Kolsky tension bar with a hollow gun barrel is that pulse shaping methods that are typically employed on Kolsky compression bar experiments can be used with little alteration. In this study, annealed C11000 copper disks with varied diameter and thickness were used as pulse shapers to achieve constant strain rates. Additionally, a pair of lock nuts was used between the threads of the tensile specimen and the bar ends to minimize the amplitude of the pseudo peak stress [3]. A tight connection between the specimen and bar ends ensured that the tensile stress wave is passed into the specimen without generating any pre-tension or torque on the specimen gage section.

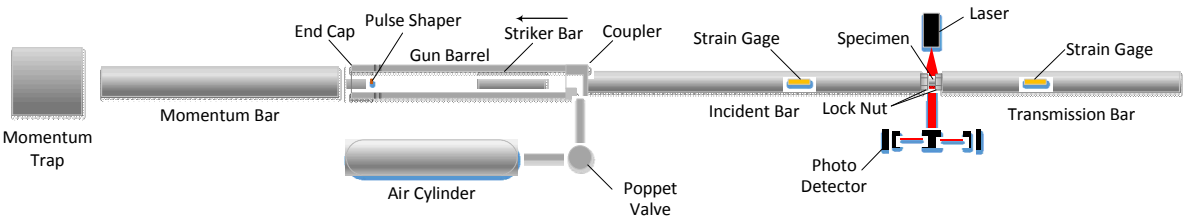

Figure 3. Kolsky tension bar setup

Following application of the dynamic tensile pulse, the specimen stress, σ, is calculated using the transmitted strain history ε_t measured on the transmission bar [5],

$$\sigma_E = E\frac{A_0}{A_s}\varepsilon_t \ , \tag{1}$$

where E and A_0 are the Young's modulus and cross-sectional area of the bar material and A_s is the specimen cross-sectional area (Equation 1). Specimen strain is calculated using the linear laser system which allows the incident and transmission bar ends to be separately tracked. Using the output of the incident and transmission bar detectors, the specimen strain is calculated as [4]

$$\varepsilon_{specimen} = \frac{L_1 - L_2}{L_s} \ , \tag{2}$$

where L_1 and L_2 are the displacements of the incident bar-specimen interface and transmission bar-specimen interface, respectively, and L_s is the specimen length (Equation 2). Inherently, the displacements L_1 and L_2 include the deformations over both gage section and transitional section (or radius) of the specimen. Therefore, Equation 2 must be corrected to only include deformation inside the gage section. A lengthy description of the strain correction is presented for this specimen geometry in Ref [5]. To summarize, based on the displacements of both ends of the specimen (L_1 and L_2) measured with the laser system, the overall engineering strain is calculated using the piecewise function based on pre and post yield, σ_y , of the specimen

$$\varepsilon_E = \begin{cases} c'\frac{L_1 - L_2}{L_s} & (\sigma \le \sigma_y) \\ \frac{L_1 - L_2 - (1-c')(L_1 - L_2)_{yield}}{L_s} & (\sigma > \sigma_y) \end{cases} \tag{3}$$

where c' is a correction factor based on the sample geometry, in this case, c' = 0.62. The strain rate history of the specimen is calculated through differentiation of the corrected engineering strain calculated using Equation 3. The dynamic tensile stress-strain curve is then determined based on the calculation of engineering stress and strain with Equations (1) and (3).

A set of typical signals from a tensile experiment at 1500 s^{-1} are shown in Fig. 4. Through pulse shaping, a nearly flat reflected pulse but with a longer rise time is generated and can be seen in Fig. 4. The longer rise time is to help the specimen achieve stress equilibrium. Equation 3 along with the laser signal is used to calculate engineering strain which is subsequently differentiated to obtain strain rate, (Fig. 5), and indicates that a constant strain rate of 1500 s^{-1} was reached after a ramp time of approximately 120 μs. Using the transmission strain gage signal and Equation 1, the engineering stress-strain curve for this experiment is plotted in Fig. 6.

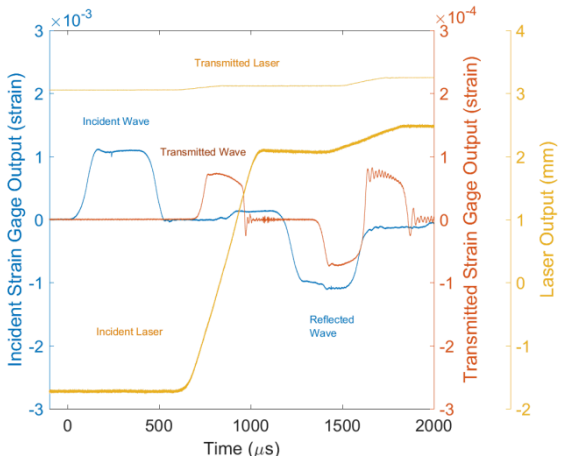

Figure 4. Original signals from a tensile experiment on 4140 steel at 1500 s^{-1}

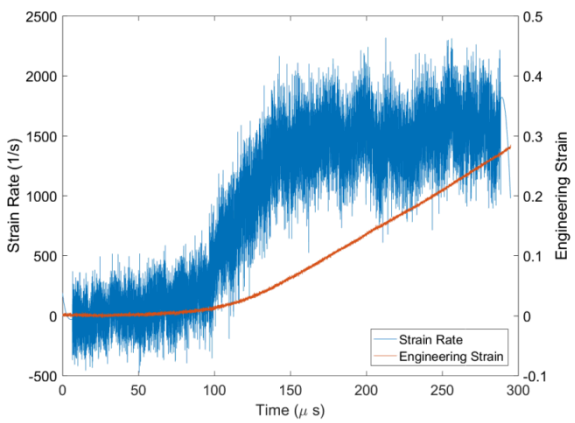

Figure 5. Strain and strain rate history

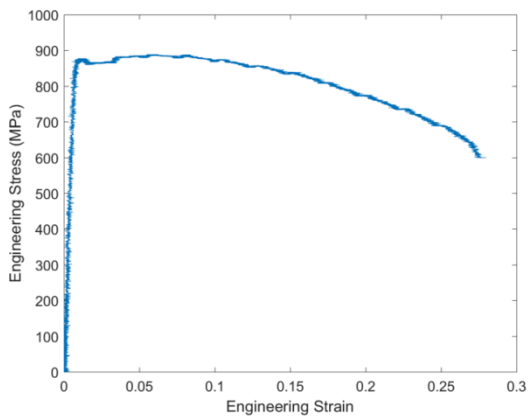

Figure 6. Tensile engineering stress-strain curve for 4140 steel at 1500 s^{-1}

After engineering tensile stress-strain curves are obtained, true stress-strain curves prior to onset of necking are calculated using the conventional method,

$$\varepsilon_{True} = \ln(1 + \varepsilon_E) \tag{4}$$

$$\sigma_{True} = \sigma_E(1 + \varepsilon_E) \tag{5}$$

where ε_E and σ_E are engineering strain and stress, respectively.

However, after the specimen is necked, equations 4 and 5 are no longer valid due to highly localized plastic deformation over the necked portion. In this study, the Bridgman correction for necking [6-8] was used to characterize the true stress and strain of each specimen at failure.

True strain is thus calculated as

$$\varepsilon_T = ln\frac{A_s}{A} \tag{6}$$

where A is the minimum of the cross-sectional area over the necked portion. The average true stress at the smallest cross-section is calculated using the engineering stress σ_E with

$$(\sigma_a)_{av} = \sigma_E \frac{A_0}{A} \tag{7}$$

Due to severe triaxiality over the necked portion, the true stress calculated with Equation (5) needs to be corrected to obtain uniaxial true stress. In this study, the following correction equation was used [7]

$$\sigma_T = k(\sigma_a)_{av} \tag{8}$$

where

$$k = \left[\left(1+\frac{4R}{D}\right) ln\left(1+\frac{D}{4R}\right)\right]^{-1} \tag{9}$$

In Equation (9), R and D are neck curvature and minimum cross-sectional diameter, respectively. Measurements of both neck curvature and necked specimen diameter were taken using a calibrated optical microscope. Typical micrographs of the measurement of the failed ends of the specimen are shown in Fig. 7.

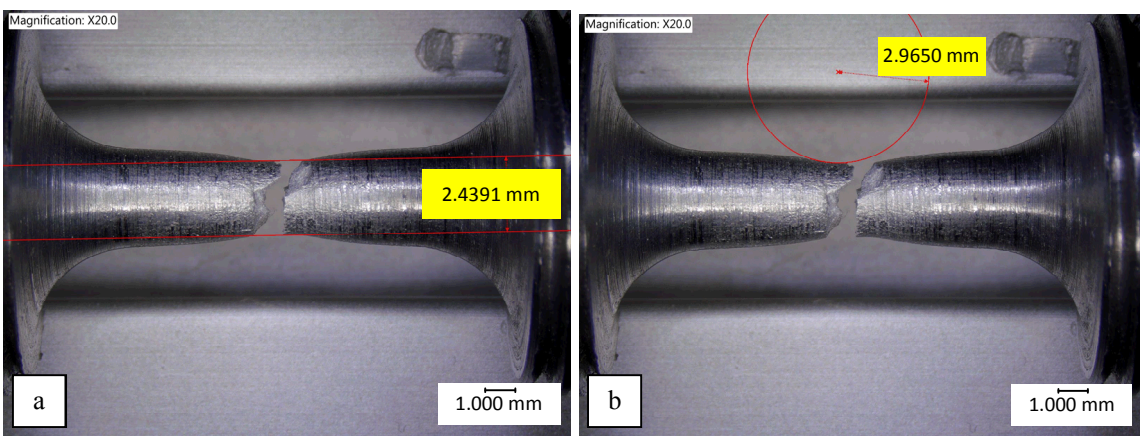

Figure 7. Optical micrograph of measurements taken using a calibrated optical microscope. a) Necked diameter measurement and b) necked radius measurement

3. Results and Discussion

Following the same data reduction procedure, the engineering stress-strain curves at three elevated strain rates for both material types were determined. The stress-strain curves were averaged for 4140 and are shown in Fig. 8a. For comparison, an average stress-strain curve at quasi-static (0.001 s^{-1}) is included in the plot, where it can be seen that an increase in yield stress of 28% was found when the strain rate increased from 0.001 s^{-1} to 3000 s^{-1}. The strain rate effects on yield strength, true failure strength, and true failure strain are shown in Fig. 8b, where the true failure stress and true failure strain were generated using the Bridgman correction (Equations 8-9). The yield strength, true failure strength, and true failure strain all increased with increasing strain rate for 4140. The average true failure

strain increased from 0.6 to 0.75 from 500 to 3000 s^{-1} while the true failure stress increased from 981.5 to 1142 MPa over the same range of strain rates.

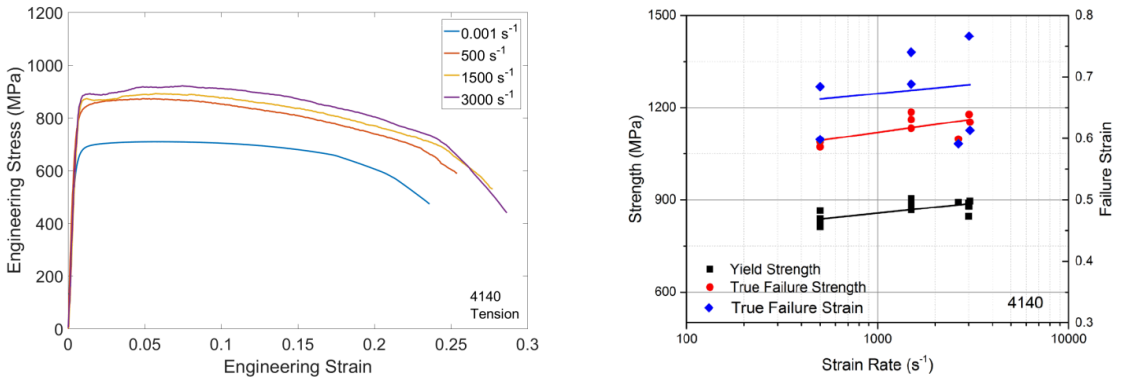

Figure 8. a) Engineering stress-strain curves at different strain rates for 4140 steel in tension b) Strain rate effects on yield strength, true failure strength, and true failure strain for 4140 steel

Averaged engineering stress-strain curves for A570 over a wide range of strain rates are shown in Fig. 9a. A570 steel exhibits an increase in yield stress of approximately 52% comparing quasi-static to 2750 s^{-1}. Due to the overall length limit of the Kolsky bar used in this study, the pulse duration was not sufficiently long to fail the A570 specimens during the first loading at a strain rate of 500 s^{-1}; hence, the end of the stress-strain curve at 500 s^{-1} shown in Fig. 9a does not represent the failure strain for those experiments. The overall shape of the engineering stress-strain curve is quite different when comparing the quasi-static and high rate responses. Most notably, when subjected to quasi-static strain rates, the engineering stress remained relatively constant until onset of diffuse necking occurred at approximately 0.27 strain prior to local necking which occurred at a strain of approximately 0.37. At high strain rates, diffuse and local necking are difficult to separate since necking occurs soon after yield. These results also clearly show that A570 is much more ductile than 4140 steel. Strain rate effects on yield stress, true failure stress, and true failure strain are shown in Fig. 9b where all parameters increased with increasing strain rate. Average true failure strain increased from 1.3 to 1.49 when the strain rate increased from 1500 to 2750 s^{-1} and the true failure stress increased from 799 to 982 MPa. Again, A570 failure stress and strain for the strain rate of 500 s^{-1} are unknown due to the limitation of the length of the Kolsky bar used in this study since those samples did not fail on the first loading pulse.

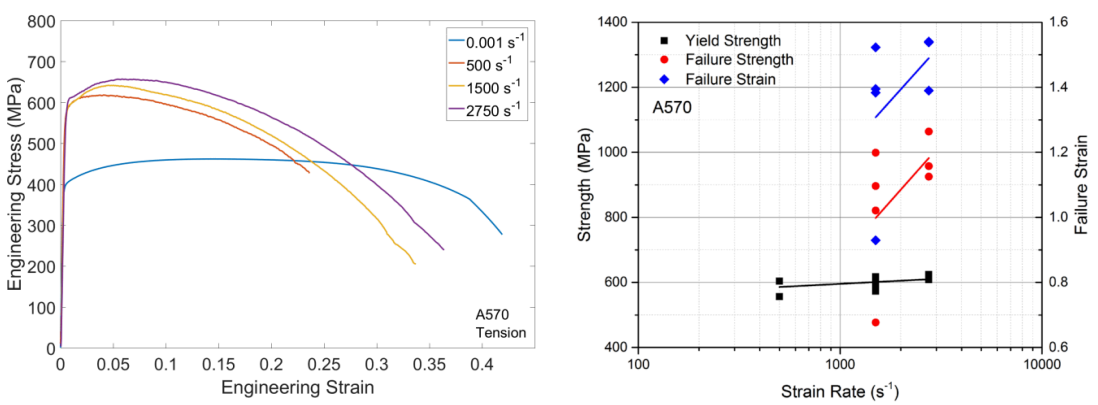

Figure 9. a) Engineering stress-strain curves at different strain rates for A570 steel in tension. b) Strain rate effects on yield strength, true failure strength, and true failure strain for A570 steel

A comparison of the true stress-strain behavior of A570 and 4140 is shown in Fig. 10. For the curves shown in Fig. 10, the true stress-strain behavior up to yield is calculated based on the averaged data from the experiment (Equations 4 and 5) and the failure stress and strain are calculated by the Bridgman correction (Equation 8 and 9). A dotted line connects the two which gives an idea of how the material behaves up to failure. While stress softening was observed in engineering stress-strain curves for A570, the data in Fig. 10 shows that A570 actually hardens until a true failure strain of approximately 1.3-1.5 is reached. Likewise for 4140, hardening is evident at elevated strain rates up until failure.

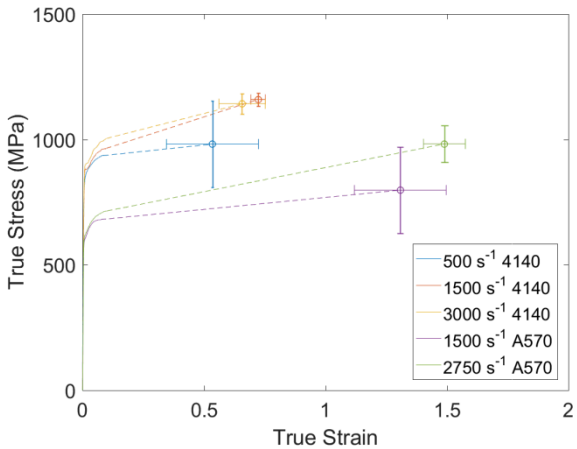

Figure 10. True stress-strain curves of A570 and 4140 showing post yield behavior. Error bars represent standard deviation of true stress and true strain at failure

4. Conclusions

A Kolsky tension bar was used to investigate the high strain rate properties of A570 and 4140 steels at strain rates of 500, 1500 and ~3000 s^{-1}. To ensure that no pseudo-stress peaks were seen in the data, lock nuts were used on each of the samples to provide good contact between the bar ends and the sample. A high speed linear laser system with dual photodetectors was used to independently track the ends of the incident and transmission bars for accurate strain measurements. The Bridgman necking correction was used to calculate the true stress and strain at failure. Both steel types showed rate sensitivity for yield strength, true failure stress, and true failure strain with increasing strain rate. For 4140, an increase in yield strength of approximately 28% was observed when comparing quasi-static strain rate to 3000 s^{-1} experiments. A570 showed an increase in yield strength of approximately 52% when the strain rate increased from quasi-static to 2750 s^{-1}. Interestingly, A570 exhibited a stress softening behavior at high strain rates that was absent from quasi-static experiments for the engineering stress-strain relation, in contrast, the true stress-strain relation for A570 indicated that the material hardened after yield. The material in this work can be utilized to generate Johnson-Cook model constants to build a strain rate sensitive constitutive model for applications that use A570 and 4140 steel.

5. Acknowledgements

Sandia National Laboratories is a multi-mission laboratory managed and operated by Sandia Corporation, a wholly owned subsidiary of Lockheed Martin Corporation, for the U.S. Department of Energy's National Nuclear Security Administration under contract DE-AC04-94AL85000.

References

[1] K. Ogawa K, Impact-tension compression test by using a split-Hopkinson bar. Exp. Mech. 24(2) (1984) 81-86
[2] B. Song B, B.R. Antoun, K. Connelly, J. Korellis, W.Y. Lu, Improved Kolsky tension bar for high-rate tensile characterization of materials. Meas Sci Tech 22 (2011) 045704.
3] B. Song, B.R. Antoun, Pseudo stress response in Kolsky tension bar experiments, Exp. Mech. 52 (2012) 525-528.
[4] X. Nie, B. Song, C.M. Loeffler, A novel splitting-beam laser extensometer technique for Kolsky tension bar experiment, J. Dynamic Behavior Mater. 1 (2015) 70-74.
[5] B. Song, P.E. Wakeland, M. Furnish, Dynamic tensile characterization of Vascomax® maraging C250 and C300 alloys, J. Dynamic Behavior Mater. 1 (2015) 153-161.
[6]. J.M. Choung, S.R. Cho, Study on the true stress correction from tensile tests. J Mech Sci Tech 22 (2008) 1039–1051
[7]. Y. Ling, Uniaxial true stress-strain after necking. AMP J Tech 5 (1996) 37–48
[8]. G. Mirone, The dynamic effect of necking in Hopkinson bar tension tests. Mech Mater 58 (2014) 84–96